Breakdown of Self-Similarity at the Crests of Large-Amplitude Standing Water Waves

Jon Wilkening*
Department of Mathematics, University of California, Berkeley, California, 94720, USA

We study the limiting behavior of large-amplitude standing waves on deep water using high-resolution numerical simulations in double and quadruple precision. While periodic traveling waves approach Stokes's sharply crested extreme wave in an asymptotically self-similar manner, we find that standing waves behave differently. Instead of sharpening to a corner or cusp as previously conjectured, the crest tip develops a variety of oscillatory structures. This causes the bifurcation curve that parametrizes these waves to fragment into disjoint branches corresponding to the different oscillation patterns that occur. In many cases, a vertical jet of fluid pushes these structures upward, leading to wave profiles commonly seen in wave tank experiments. Thus, we observe a rich array of dynamic behavior at small length scales in a regime previously thought to be self-similar.

Singularities in fluid mechanics are generally expected to be asymptotically self-similar [1]. These can be dynamic singularities, such as bubble pinch-off [2] or wave breaking [3], or parametric singularities, where a family of smooth solutions terminates at a singular solution. A famous example of the latter type was posed by Stokes in 1880, who used an asymptotic expansion of the stream function to argue that the periodic traveling water wave of greatest height should have an interior crest angle of 120°. This crest angle has been confirmed in numerous computational studies [4] as well as theoretically [5]. The asymptotic behavior of the almost highest traveling wave was analyzed by Longuet-Higgins and Fox [6, 7].

Because genuine dynamics are involved, existing numerical methods have been unable to maintain the accuracy needed to fully explore the limiting behavior of large-amplitude standing waves. As a result, Penney and Price's conjecture [8] that a limiting standing wave exists and develops 90° interior crest angles each time the fluid comes to rest has remained open since 1952. Such a singularity would be both dynamic and parametric. The standing waves in question are spatially periodic and have zero impulse (horizontal momentum), maintaining even symmetry for all time. They are also temporally periodic, alternately passing through two zero-velocity rest states of maximal potential energy.

Small-amplitude standing waves of this type were proved to exist by Iooss, Plotnikov, and Toland [9]. Larger-amplitude waves were computed by Mercer and Roberts [10], who discovered that the wave steepness (half the crest-to-trough height) does not increase monotonically over the entire one-parameter family of standing waves. They proposed using (downward) crest acceleration, A_c, as a continuation parameter instead. We reproduce (and extend) their plot of wave steepness versus crest acceleration in Fig. 1. Since pressure increases with depth near the free surface [11], Euler's equations imply that A_c cannot exceed g, the acceleration of gravity.

Taylor [12] performed wave tank experiments and confirmed that large-amplitude standing waves do form reasonably sharp crests close to 90 degrees. A further increase in amplitude caused the waves to splash and become unstable in the transverse direction. Grant [13] and Okamura [14] have written theoretical papers to support the 90° conjecture. Okamura also performed numerical experiments [15, 16] to back this claim. Extrapolating from numerical solutions, Mercer and Roberts [10] speculated that the limiting crest angle might be as sharp as 60°. Schultz et. al. [17] also predicted a limiting wave profile with a crest angle smaller than 90° and offered the possibility that a cusp may form instead of a corner.

Our objective is to challenge the assumption that standing waves behave as traveling waves in their approach of an "extreme" limiting wave. If there is no limiting wave profile, then a local analysis suggesting a geometric singularity (corner or cusp) is inapplicable.

The equations of motion for a two-dimensional irrotational ideal fluid of infinite depth are

$$\eta_t = \phi_y - \eta_x \phi_x, \tag{1a}$$

$$\Phi_t = P\left[\phi_y \eta_t - \tfrac{1}{2}|\nabla\phi|^2 - g\eta\right], \tag{1b}$$

where $\eta(x,t)$ is the upper boundary of the evolving fluid and $\Phi(x,t) = \phi(x,\eta(x,t),t)$ is the restriction of the velocity potential to the free surface. Both $\eta(x,t)$ and $\Phi(x,t)$ are assumed to be 2π periodic in x. In (1b), P is the or-

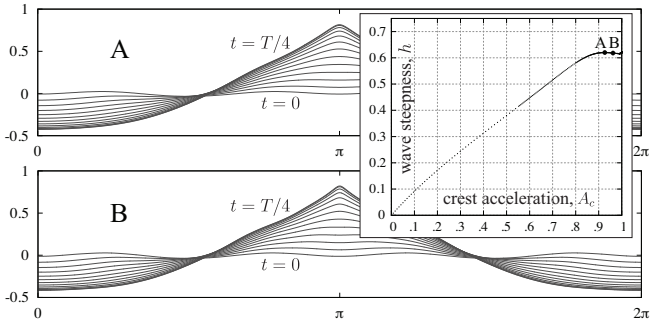

FIG. 1. Bifurcation diagram and selected standing waves, plotted at equal time slices over a quarter period. The wavelength is taken to be 2π, and $g = 1$. The crest tip sharpens as A_c increases over the range $0 \le A_c \le 0.985$, where previous numerical studies are reliable. In particular, the curvature at the crest is visibly higher for solution B than for A.

thogonal projection to zero mean. This equation comes from $\Phi_t = \phi_t + \phi_y \eta_t$ and the unsteady Bernoulli equation $\phi_t + \frac{1}{2}|\nabla\phi|^2 + \frac{p}{\rho} + gy = c(t)$, where the arbitrary constant $c(t)$ is chosen to preserve the mean of $\Phi(x,t)$.

To evaluate the right-hand side of (1) for the purpose of time stepping, we use a boundary integral collocation method. Details will be given elsewhere [18]. Briefly, we represent ϕ at a point $z = x + iy$ in the fluid using a double layer potential. Suppressing t in the notation and summing over periodic images [19], the result is

$$\phi(z) = \frac{1}{2\pi} \int_0^{2\pi} \widetilde{K}(z,\alpha)\mu(\alpha)\, d\alpha, \tag{2}$$

where $\widetilde{K}(z,\alpha) = \mathrm{Im}\left\{\frac{\zeta'(\alpha)}{2} \cot\left(\frac{z-\zeta(\alpha)}{2}\right)\right\}$. A prime represents a derivative with respect to α, and

$$\zeta(\alpha) = \xi(\alpha) + i\eta(\xi(\alpha)) \tag{3}$$

is a parametrization of the curve. The change of variables $x = \xi(\alpha)$ allows for smooth mesh refinement near the crest tip. Letting z approach the boundary, we obtain a second-kind Fredholm integral equation for μ:

$$\Phi(\xi(\alpha)) = \frac{\mu(\alpha)}{2} + \frac{1}{2\pi} \int_0^{2\pi} K(\alpha,\beta)\mu(\beta)\, d\beta, \tag{4}$$

$$K = \mathrm{Im}\left\{ \frac{\zeta'(\beta)}{2} \cot\left(\frac{\zeta(\alpha)-\zeta(\beta)}{2}\right) - \frac{1}{2}\cot\left(\frac{\alpha-\beta}{2}\right)\right\}.$$

Once $\mu(\alpha)$ is known, we compute ϕ_x and ϕ_y on the boundary from (2), closing the system (1); see [18].

We discretize space and time adaptively to resolve the solution as it becomes increasingly singular. Time is divided into ν segments $\theta_l T$, where $\theta_1 + \cdots + \theta_\nu = 1/4$ and T is the current guess for the period. On segment l, we fix the number of (uniform) time steps, N_l, the number of spatial grid points, M_l, and the function

$$\xi_l(\alpha) = \int_0^\alpha E_l(\beta)\, d\beta, \quad E_l(\alpha) = 1 - P\left[A_l \sin^4(\alpha/2)\right],$$

which controls the grid spacing in the change of variables $x = \xi_l(\alpha)$. A_l is a parameter chosen between 0 (uniform spacing) and 8/5, the value where $\xi_l(\alpha)$ ceases to be a diffeomorphism. As before, P projects out the mean.

To compute standing waves, we use the Levenberg-Marquardt method [20], a trust-region algorithm for nonlinear least squares problems, to minimize

$$f(c) = \frac{1}{4\pi} \int_0^{2\pi} \Phi(x, T/4)^2\, dx, \qquad c \in R^{n+1}, \tag{5}$$

where c contains the period as well as the nonzero Fourier modes of the initial conditions; i.e., $T = c_0$ and

$$\hat{\eta}_k(0) = c_{|k|} \quad (k \text{ odd}), \qquad \hat{\Phi}_k(0) = c_{|k|} \quad (k \text{ even}). \tag{6}$$

Here k ranges from $-n$ to n, excluding 0, and n is chosen to be close to $\frac{1}{4}M_1$, leaving the upper half of the spectrum of η and Φ to be zero initially. A symmetry argument [10] shows that driving the velocity potential to zero at time $T/4$ with initial conditions of the form (6) leads to a standing wave with period T and zero impulse. The method fails if f reaches a nonzero local minimum.

We discretize (5) with spectral accuracy by redefining $f = \frac{1}{2} r^T r$, where $r \in \mathbb{R}^m$, $m = M_\nu$, and

$$r_i = \Phi(\xi_\nu(\alpha_i), T/4)\sqrt{E_\nu(\alpha_i)/m}, \qquad \alpha_i = 2\pi i / M_\nu.$$

The square root comes from $dx = E_\nu(\alpha)\, d\alpha$. Typically, $4n \le m \le 10n$. To track families of solutions, one of the c_k is chosen as a continuation parameter [21] and eliminated from the search space when minimizing f. When a turning point is detected in this c_k, we switch to a different one; see [18, 19] for details. The Jacobian $J_{ik} = \partial r_i / \partial c_k$ is computed by solving the linearization of (1) about the current solution to obtain $\frac{\partial}{\partial c_k}\Phi(x, T/4)$. This can be parallelized very efficiently [18], dramatically increasing the resolution we are able to achieve.

Our results are summarized in Figs. 2 and 3. First, we corroborate the result of Mercer and Roberts [10] that wave steepness, h, reaches a local maximum of $h_{\max} = 0.62017$ at $A_c = 0.92631$. (The values reported in [10] were 0.6202 and 0.9264.) Using quadruple precision, we are able to compute $h_{\max}$ to 26 digits of accuracy and the corresponding A_c to 13 digits. Okamura [15], who found that h increases monotonically all the way to $A_c = 1$, was incorrect. Second, we find that crest acceleration has turning points at $A_c = 0.99135$ and 0.99040. This is a surprise, as A_c was chosen as a continuation parameter in [10] to avoid the lack of monotonicity in h. In our work, h and A_c are plotted parametrically as

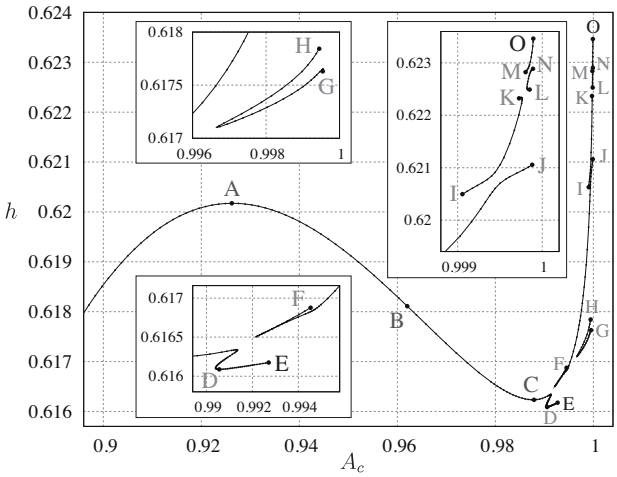

FIG. 2. The bifurcation curve in Fig. 1 becomes fragmented in the range $0.985 < A_c < 1$, where previous numerical studies break down. The labels A–O correspond to wave profiles shown in Fig. 3. The turning point in wave steepness at C, the lack of monotonicity in A_c, the complicated branching structure, and the existence of standing waves with $h > 0.62017$ were not previously known.

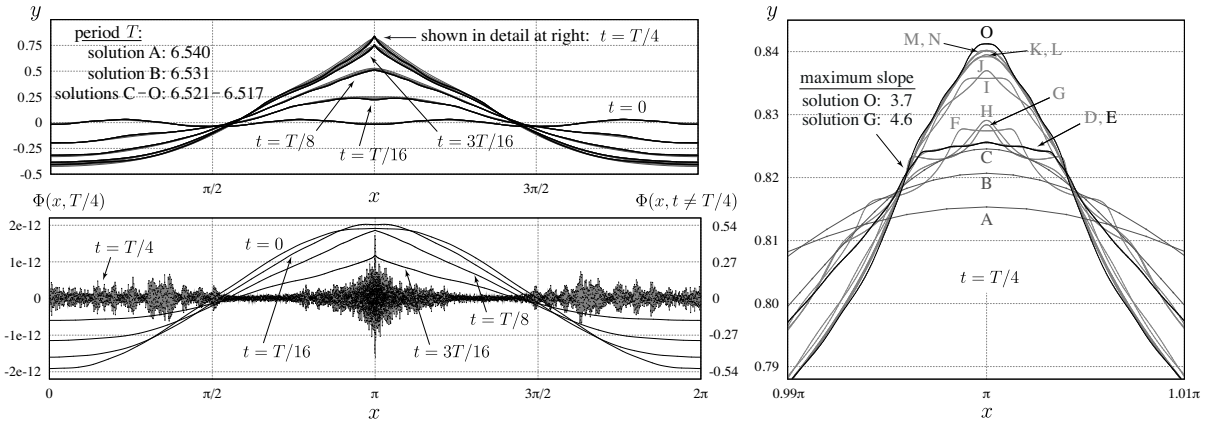

FIG. 3. Evolution of standing waves and velocity potential over a quarter period. (Top left) Solutions A–O in Fig. 2 are plotted on top of each other at the indicated times. (Right) These solutions develop oscillatory structures near the crest that change phase across disconnections in the bifurcation diagram. Solutions D–O have 350–600 grid points between 0.99π and 1.01π. With at most 3 grid points in this interval, previous numerical studies could not resolve these structures. (Bottom left) The velocity potential of solution O has been driven almost to zero at $t = T/4$, yielding $f = 1.3 \times 10^{-26}$. For this solution, we used $\nu = 4$, $\theta_l = \{0.2, 0.2, 0.4, 0.2\}$, $M_l = \{4608, 6144, 6912, 8192\}$, $N_l = \{192, 288, 768, 480\}$, and $A_l = \{0, 0.774, 1.358, 1.381\}$.

functions of whichever c_k is currently used as a continuation parameter. Finally, in the process of tracking this primary branch of solutions, we discovered several other families of standing waves. Each of these branches was tracked in both directions until the computations became too expensive to continue further with the desired accuracy, $f \sim 10^{-26}$ in double precision.

The standing waves that constitute these branches look qualitatively similar to each other in the large, where they closely resemble the photographs from Taylor's wave tank experiments [12]. However, as illustrated in Fig. 3, solutions on different branches feature different oscillation patterns in the vicinity of the crest tip. The rapid increase in wave steepness from solution E to solution O in Fig. 2 corresponds to a vertical jet of fluid that forms near the crest before the standing wave reaches its rest state. The resulting protrusion causes the maximum slope to be much larger than 1 for most of these solutions. Taylor photographed similar structures at the crest in his wave tank experiments. Schultz et. al. [17] argued that surface tension was responsible for these protrusions, but we find that they occur even without surface tension. Comparing solutions A–E on the primary branch, we see that solutions eventually flatten out at the crest and become oscillatory rather than sharp. Figure 4 provides further evidence that these oscillations grow large enough to prevent this family of solutions from approaching a limiting wave profile in an asymptotically self-similar fashion.

Regarding accuracy, our method is spectrally accurate in space, 8th or 15th order in time [18], and quadratically convergent in the search for a minimizer of f in (5). We achieve robustness by formulating the shooting method as an overdetermined nonlinear least squares problem. If the numerical solution loses resolution, the equations $r_i(c) = 0$ become incompatible with each other and the objective function $f = \frac{1}{2} r^T r$ grows accordingly. This prevents the method from giving misleading overestimates of the accuracy of the standing waves it finds. For example, we recomputed solution O of Fig. 3 in quadruple precision on a finer mesh ($M_l = \{6144, 7500, 8192, 9216\}$, $\theta_l = \{0.1, 0.3, 0.4, 0.2\}$, and $A_l = \{0, 1.043, 1.405, 1.476\}$), using the initial conditions obtained by minimizing f in double precision. The more accurately computed value of f is 8.6×10^{-27}, which is 34% smaller than predicted in double precision. This level of inaccuracy in the predicted error is acceptable, as driving $\Phi(x, T/4)$ to zero entails eliminating as many significant digits as possible. For solution A, we repeated the minimization in quadruple precision, causing f to decrease from 2.2×10^{-28} to 2.1×10^{-60}. In addition to f, we monitor energy conservation and the decay of Fourier modes at various times to ensure that η and Φ remain resolved to machine precision; see [18] for more details.

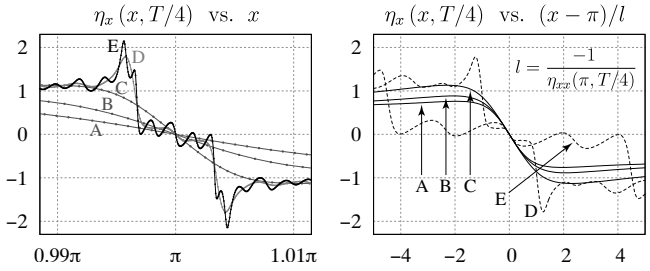

FIG. 4. Breakdown of self-similarity on the primary branch. When lengths are rescaled so the radius of curvature at the crest is 1, the slopes of solutions A–C have similar shapes. In the traveling case (Fig. 5), these rescaled slopes would approach a limiting curve. But, for standing waves, oscillations develop, and a limiting curve does not emerge.

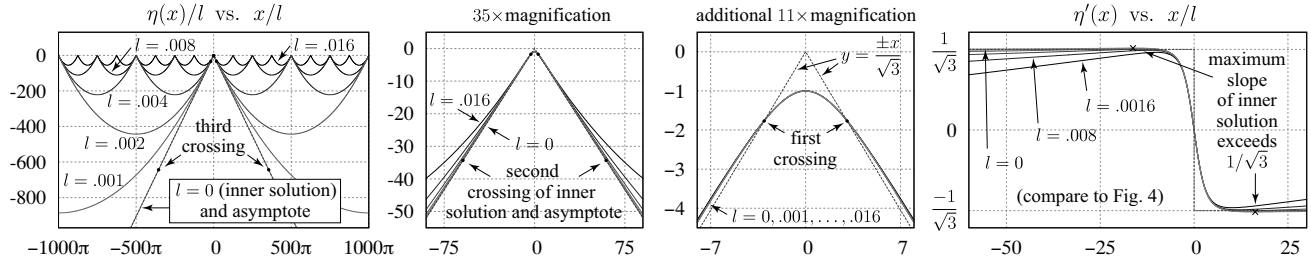

FIG. 5. Self-similar asymptotics of traveling water waves near the wave crest. (Left) Using a variant of our standing wave code, we computed 5 periodic traveling solutions with wavelength 2π and particle speed q at the wave crest, chosen so that $l = q^2/2g$ has the values shown. We then plotted $\eta(x)/l$ versus x/l, as well as the inner solution of [6]. The distance between successive crossings of the inner solution with its asymptote grows exponentially; thus, l must be extremely small to observe oscillatory behavior near the crest. (Right) As $l \to 0$, the slopes of the rescaled periodic waves approach the slope of the inner solution.

It is instructive to compare our results to the traveling wave case. Longuet-Higgins and Fox [6, 7] showed that periodic traveling waves are asymptotically self-similar in two scaling regimes. If the wavelength, L, is held fixed as the crest tip sharpens, the limiting wave profile has a 120° corner. This is the outer solution of [7], predicted by Stokes and proved to exist in [5]. If, instead, the fluid velocity at the crest remains fixed as the wavelength goes to infinity, the limiting wave profile is shown in Fig. 5. This inner solution crosses the asymptotes $y = \pm x/\sqrt{3}$ infinitely often [6], implying that traveling waves approach Stokes's limiting wave in an oscillatory manner, rather than monotonically, with L fixed.

The oscillations in the standing wave case are of a completely different nature. No choice of scaling will cause the curves in Fig. 4 to approach a limiting inner solution. We believe these oscillations are caused by resonant modes in the two-point boundary value problem (1) with boundary conditions $\Phi(x, \pm T/4) = 0$, treating T as a bifurcation parameter. A resonant mode is a perturbation that nearly satisfies the linearized boundary value problem. Such modes can be strongly excited in the process of computing standing waves, especially in finite depth [18, 22, 23]. Disconnections in the bifurcation diagram seem to occur when a resonant mode can be excited with more than one amplitude. For example, solutions I and J in Fig. 3 both contain a secondary, higher-frequency standing wave (the resonant mode) superimposed on a low-frequency carrier wave. The secondary wave sharpens the crest at J and flattens it at I, being 180 degrees out of phase from one branch to the other.

We conclude that resonance is responsible for oscillations and trumps self-similarity in determining the dynamics of standing waves at small scales. This shows that, although under-resolved numerical simulations may exhibit self-similar dynamics, as happened in [15], the true dynamics may be more complex. Recent work on singularity formation in free surface flow problems, such as droplet and bubble pinch-off [1, 2] and wave breaking [3], may also benefit from higher-resolution simulations, which could reveal new aspects of their dynamics.

This research was supported by the National Science Foundation (DMS-0955078) and the U.S. Department of Energy (DE-AC02-05CH11231). The computations were performed on the Lawrencium cluster at LBNL.

* wilken@math.berkeley.edu

[1] J. Eggers and M. A. Fontelos, Nonlinearity **22**, R1 (2009).
[2] K. S. Turitsyn, L. Lai, and W. W. Zhang, Phys. Rev. Lett **103**, 124501 (2009).
[3] T. J. Bridges, Nonlinearity **22**, 947 (2009).
[4] I. S. Gandzha and V. P. Lukomsky, Proc. R. Soc. A **463**, 1597 (2007).
[5] C. J. Amick, L. E. Fraenkel, and J. F. Toland, Acta Math. **148**, 193 (1982).
[6] M. S. Longuet-Higgins and M. J. H. Fox, J. Fluid Mech. **80**, 721 (1977).
[7] M. S. Longuet-Higgins and M. J. H. Fox, J. Fluid Mech. **85**, 769 (1978).
[8] W. G. Penney and A. T. Price, Phil. Trans. R. Soc. London A **244**, 254 (1952).
[9] G. Iooss, P. I. Plotnikov, and J. F. Toland, Arch. Rat. Mech. Anal. **177**, 367 (2005).
[10] G. N. Mercer and A. J. Roberts, Phys. Fluids A **4**, 259 (1992).
[11] S. Wu, Invent. Math. **130**, 39 (1997).
[12] G. I. Taylor, Proc. Roy. Soc. A **218**, 44 (1953).
[13] M. A. Grant, J. Fluid Mech. **60**, 593 (1973).
[14] M. Okamura, Wave Motion **28**, 79 (1998).
[15] M. Okamura, Wave Motion **37**, 173 (2003).
[16] M. Okamura, J. Fluid Mech. **646**, 481 (2010).
[17] W. W. Schultz, J.-M. Vanden-Broeck, L. Jiang, and M. Perlin, J. Fluid Mech. **369**, 253 (1998).
[18] J. Wilkening and J. Yu, (in preparation).
[19] D. M. Ambrose and J. Wilkening, Proc. Nat. Acad. Sci. **107**, 3361 (2010).
[20] J. Nocedal and S. J. Wright, *Numerical Optimization* (Springer, New York, 1999).
[21] H. B. Keller, *Numerical methods in bifurcation problems* (Springer, New York, 1987).
[22] G. N. Mercer and A. J. Roberts, Wave Motion **19**, 233 (1994).
[23] D. H. Smith and A. J. Roberts, Phys. Fluids **11**, 1051 (1999).